

# An explicit multistep method for the Wigner problem

Yunfeng Xiong \*

(Department of Mathematics, Zhejiang University, Hangzhou 310027, Zhejiang, P.R.China)

**Abstract:** In this paper, an explicit multistep scheme is proposed for solving the initial-value Wigner problem, by approximating its integrated form using extrapolation polynomials. The pseudo-differential operator is tackled by the spectral collocation method. The time stepping of multistep scheme is not restricted by any CFL-type condition, as the hyperbolic operator is not approximated by finite difference methods. It is demonstrated that the calculations of the Wigner potential can be carried out by two successive FFTs, thereby reducing the computational complexity dramatically. Numerical examples illustrating its accuracy are presented.

**Keywords:** Wigner equation; spectral collocation method; Adams multistep scheme; quantum transport.

## 1 Introduction

The progressive miniaturization of semiconductor devices, and the use of bulk materials other than silicon, necessitate the use of a wide variety of model in semiconductor device simulation [1]. Among various of quantum mechanical models, the Wigner representation [2] is a useful tool to describe the quantum transport of charged particles in a solid state medium. Although it is not a real probability function, due to possible negative values, the Wigner function serves the role of a distribution [3]. Hence it is able to predict macroscopically measurable quantities, such as currents and heat fluxes. Recently, the Wigner function is also widely applied in non-equilibrium quantum statistical mechanics, optics and information theory [3, 4].

Numerical methods for solving the Wigner problem have been greatly developed in past few decades. The first-order upwind finite difference method (FDM) was first employed by Frensley to simulate the resonant tunneling diode (RTD), with the inflow boundary conditions in open quantum system [5]. This was then adapted by Ringhofer, by introducing the spectral collocation method to discretize the pseudo-differential operator [6]. The operator splitting scheme, first used by plasma physicists to study the Landau damping of quantum system [7], was generalized to the Wigner-Poisson system and analyzed thoroughly by Arnold and Ringhofer [8]. Several advanced numerical techniques, like adaptive mesh and numerical conservative laws, were also employed in solving the linear collisionless Wigner equation [4].

However, solving the high dimensional Wigner problem through grid-based methods is still problematic, due to the dramatic growth of sampling points in full phase space [9]. It will also cause severe numerical errors when treating the hyperbolic operator by finite difference techniques, since the Wigner function oscillates rapidly in phase space [10, 11]. In recent years, a particle-based approach, termed the Particle Monte Carlo (PMC) method, has burgeoned with the developments of the particle affinity and effective quantum potential [12]. The PMC method doesn't suffer from the problem connected to the diffusion term. Besides, it

---

\* Email addresses: xiongyf@zju.edu.cn.

allows parallel and distributed implementation, thereby facilitating the device simulations of electron-electron interactions in three dimension [13]. On the other hand, the particle-based methods may have some inherent statistical noise, due to the use of finite number of super-particles. Therefore, it necessitates an efficient grid-based numerical solver, along with a proper treatment of the hyperbolic operator.

An appropriate formulation of boundary conditions is a major problem in the application of Wigner model. The inflow boundary conditions have been reported to cause spurious numerical reflections of outgoing wave packets [14], which can be resolved by absorbing boundary conditions [15]. In particle-based methods, the setting of affinity introduces absorbing boundary conditions in a very easy fashion. For the coupled Wigner-Poisson problem, it's not trivial to devise a reasonable boundary condition for the self-consistent electrostatic field, since it should be chosen from the requirement that the system asymptotically approach charge neutrality. Until recently, there is not a systematic study on how to formulate the boundary condition for the electrostatic field in grid-based Wigner solvers. In fact, the original Wigner equation is a Cauchy problem, thus one should handle unphysical phenomena carefully when introducing an artificial boundary condition. An ideal grid-based solver should be devised for an initial-value problem and compatible with different types of boundary conditions.

The main purpose of this paper is to derive an explicit multistep scheme for the initial-value Wigner problem, which is an extension of semi-Lagrangian scheme [16]. It exploits the  $C_0$ -semigroup generated by the diffusion term, instead of approximating it by finite difference techniques. The intuition comes from the fact that the Wigner equation can be represented as an abstract ODE, therefore several multistep ODE solvers might be adapted to deal with the quantum transport. The smooth part of the pseudo-differential operator is tackled by the spectral collocation method, while the collision term is approximated by numerical integration techniques. It is demonstrated that the cost of computing the Wigner potential can be reduced dramatically via Fast Fourier transformation, thereby facilitating its application in high-dimensional case. In addition, an explicit scheme allows parallel and distributed computing, since all the calculations can be carried out independently. The accuracy of the multistep scheme is illustrated by simulating the motion of a Gaussian wave packet in several potential barriers, that has been studied in [4].

The rest of the paper is organized as follows. In Section 2, the Wigner equation and the modeling of quantum transport are briefly reviewed. The explicit multistep scheme for the Wigner problem is demonstrated in Section 3, along with the spectral collocation method. Numerical results are illustrated in Section 4, with a concluding remark given in Section 5.

## 2 An introduction to the Wigner equation

We briefly review the Wigner equation and several models of quantum plasma. For convenience, we adopt the same notations as in [1]. Our discussion is independent of the dimension  $d$  ( $d = 1, 2, 3$ ), since the Wigner equation allows a reduction in dimension.

The Wigner function  $w(x, k, t)$  is defined by the Weyl-Wigner transformation of the density matrix for

mixed states [1, 3],

$$\begin{aligned}\rho(r, s, t) &= \sum_j \rho(\omega_j) \psi_j(r, t)^* \psi_j(s, t), \\ w(x, k, t) &= (2\pi)^{-d} \int_{\mathbb{R}^d} d\eta \rho\left(x + \frac{\eta}{2}, x - \frac{\eta}{2}, t\right) e^{-i\eta \cdot k},\end{aligned}\tag{1}$$

which satisfies the Fourier transformed quantum Liouville equation, referred to as the (collisionless) Wigner equation

$$\begin{aligned}\partial_t w + \frac{\hbar}{m} k \cdot \nabla_x w + \theta[V] w &= 0, \\ \theta[V] &= \delta V\left(x, \frac{1}{2i} \nabla_k\right), \quad \delta V\left(x, \frac{\eta}{2}\right) = V\left(x + \frac{\eta}{2}\right) - V\left(x - \frac{\eta}{2}\right),\end{aligned}\tag{2}$$

where  $\hbar$  is the reduced Planck constant and  $\theta[V]$  is termed pseudo-differential operator. It is convenient to derive the spectral representation of pseudo-differential operator through the Stone-Weierstrass theorem.

An equivalent representation of  $\theta[V]$  is given by

$$\theta[V] w(x, k, t) = (2\pi)^{-d} \int_{\mathbb{R}^d} d\tilde{k} \int_{\mathbb{R}^d} d\eta \frac{i}{\hbar} \delta V\left(x, \frac{\hbar}{2} \eta, t\right) w(x, \tilde{k}, t) \exp(i\eta \cdot (k - \tilde{k})),\tag{3}$$

In practice, Eq.(3) is usually approximated by numerical integration techniques.

In modeling the electron plasma in metal, however, it is necessary to include the scattering processes of electrons with phonons quantum mechanically [17]. The Levinson's formalism of interaction terms properly introduces the intracollisional field effect, while the transformation is entirely nontrivial [18]. In the real simulations, there are two approaches to formulating the scattering effect, namely, the relaxation time model and the Fokker-Planck model.

The relaxation time model is expressed as

$$Q(w) = \frac{1}{\tau} \left( \frac{n}{n_0} w_0 - w \right), \quad n(x, t) = \int_{\mathbb{R}^d} dk w(x, k, t), \quad n_0(x, t) = \int_{\mathbb{R}^d} dk w_0(x, k),\tag{4}$$

which lumps all dissipation process into one macroscopic parameter: the relaxation time  $\tau$ .

The Fokker-Planck term model is given by

$$Q(w) = \frac{1}{\tau} \text{div}_k \left( \frac{mT_0}{\hbar^2} \nabla_k w + kw \right),\tag{5}$$

where  $T_0$  denote the lattice temperature.

In addition, it is reasonable to include the self-consistent electrostatic potential in simulating RTDs, which be achieved by coupling Eq.(2) with a Poisson equation

$$\Delta_x V^{self}(x, t) = \int_{\mathbb{R}^d} dk w(x, k, t) - D(x),\tag{6}$$

where  $D(x)$  denotes the doping concentration.

After changing the time scale (let  $\frac{\hbar}{m} = 1$ ), we arrive at the reduced collisional Wigner-Poisson equation, the quantum analogue to the Vlasov-Poisson model [19],

$$\begin{aligned} \partial_t w + k \cdot \nabla_x w + \theta[V] w &= Q(w), \quad \theta[V] = V \left( x + \frac{1}{2i} \nabla_k \right) - V \left( x - \frac{1}{2i} \nabla_k \right), \\ V &= V^{ext} + V^{self}, \quad \Delta_x V^{self}(x, t) = \int_{\mathbb{R}^d} dk w(x, k, t) - D(x), \\ Q(w) &= \frac{1}{\tau} \left( \frac{n}{n_0} w_0 - w \right), \quad w(x, k, 0) = w_0(x, k). \end{aligned} \quad (7)$$

The existence and uniqueness of a global classical solution of collisionless Wigner-Poisson equation (namely, ignoring  $Q(w)$  term) is given by Brezzi and Markowich [20], via the reformulation of the quantum transport problem as a system of countably many Schrödinger equations coupled to a Poisson equation. For more details of Wigner function, one can refer to [3].

### 3 Numerical scheme

In this section, we mainly discuss the numerical scheme of solving Eq.(7). It is observed that the second term (the diffusion term) is a simple hyperbolic operator, while the pseudo-differential operator is nonlocal and does not possess classical characteristics. Traditional numerical scheme can be roughly summarized as the following three steps:

- (1) Transform Eq.(7) into a hyperbolic system through discretization in  $k$ -direction;
- (2) Use the finite difference method to discretize the hyperbolic operator  $k \cdot \nabla_x$ ;
- (3) Use an implicit-explicit ODE solver to integrate the reduced dynamical system.

The reduced dynamical system is usually a multiscale problem. Therefore an implicit treatment of the hyperbolic operator is much more preferred, for it's more stable in stiff case and allows a longer time step. The pseudo-differential operator is discretized by other methods explicitly, such as the spectral collocation method and the numerical integration formula. Then it remains to solve a linear equation by Newton methods.

For high dimensional problems, however, the number of grid points increases dramatically and the coefficient matrix is extremely large. It is also found that the Wigner function oscillates rapidly in phase space, where quantum interference is dominant. The step size in  $x$ -direction must be sufficiently small, otherwise severe numerical errors will be observed. Therefore, the explicit methods, with a proper treatment of the hyperbolic operator, are much more useful in solving the high dimensional problem owing to their lower computational complexity.

An alternative way of solving Eq. (7) is derived from its integrated form (or the mild solution). Under the spectral representation, the reduced hyperbolic system can be represented as an abstract ODE system in the light of operator semigroup theory. If the integrand is a continuous function with respect to  $t$ , it is reasonable to use interpolation or extrapolation polynomials to approximate the integral. Before discussing the explicit multistep scheme, we first turn to the spectral representation of the Wigner equation.

## A. Spectral collocation method

The spectral collocation method, proposed by Ringhofer [1, 6], is based on the fact that the plane waves are the eigenfunctions of the pseudo-differential operator associated with the smooth Wigner potentials. It has been demonstrated the spectral collocation method is well-posed and convergent [6], with the assumption that  $w$  and  $V(x)$  have sufficient regularities and  $w(x, k, t)$  has a compact support.

Following Ringhofer, assume that  $w(x, k, t)$  has a compact support in  $k \in \left[-\frac{\pi}{\alpha}, \frac{\pi}{\alpha}\right]^d$ , then we can approximate the Wigner function by trigonometric polynomial of the form (in  $L^2$  space)

$$w \approx w_N(x, k, t) = \sum_{n \in \mathbb{N}} c(x, n, t) \phi_n(k). \quad \mathbb{N} = \{-N, \dots, N\}^d, \quad N = 2^m \quad (8)$$

The plane wave basis is given by

$$\phi_n(k) = \left(\frac{\alpha}{2\pi}\right)^{d/2} \exp(i\alpha n \cdot k), \quad (9)$$

which satisfies

$$\int_{\left[-\frac{\pi}{\alpha}, \frac{\pi}{\alpha}\right]} \phi_m^* \phi_n = \delta(m-n), \quad (\Delta k)^d \sum_{s \in \mathbb{N}} \phi_m(k_s)^* \phi_n(k_s) = \delta_N(m-n), \quad (10)$$

where  $\delta_N$  is a Kronecker  $\delta$  with period  $N$ ,  $\Delta k = \frac{\pi}{N\alpha}$  and  $k_s = \frac{s\pi}{N\alpha}$ .

Since

$$c(x, n, t) = (\Delta k)^d \sum_{s \in \mathbb{N}} \phi_n^*(k_s) w_N(x, k_s, t), \quad (11)$$

$\theta[V]w$  can be approximated by

$$B(x, k_m, t) = \theta[V]w_N(x, k_m, t) = i \frac{(\Delta k)^d}{\hbar} \sum_{n \in \mathbb{N}} \sum_{s \in \mathbb{N}} \delta V\left(x, \frac{\alpha \hbar}{2} n, t\right) w_N(x, k_s, t) \phi_n^*(k_s) \phi_n(k_m), \quad (12)$$

where  $B$  is called a tensor matrix.

When an explicit scheme is used, the computation of tensor matrix  $B$  can be carried out by two successive FFTs, for

$$B(x, k_m, t) = \theta[V]w_N(x, k_m, t) = i \frac{(\Delta k)^d}{\hbar} \sum_{n \in \mathbb{N}} \left[ \sum_{s \in \mathbb{N}} w_N(x, k_s, t) \phi_n^*(k_s) \right] \delta V\left(x, \frac{\alpha \hbar}{2} n, t\right) \phi_n(k_m). \quad (13)$$

For simplicity, we assume  $d = 1$ . Denote by

$$\begin{aligned} H_n &= \sum_{s=-N}^N w(x, k_s, t) e^{-in \cdot k_s} = \sum_{s=-N}^N w(x, k_s, t) e^{-2\pi i \frac{ns}{2N}}, \quad n = -N+1, \dots, N \\ H_{-N} &= \sum_{s=-N}^N w(x, k_s, t) e^{s\pi i}. \end{aligned} \quad (14)$$

A simple calculation yields

$$H_n = \sum_{s=0}^{2N-1} w(x, k_s, t) e^{-2\pi i \frac{ns}{2N}} + w(x, k_{-N}, t) e^{in\pi}, \quad (15)$$

where  $k_s = k_{s-2N}$  ( $s = N + 1, \dots, 2N - 1$ ). Thus, the first term in the right-hand side can be performed by standard FFT program.

It remains to calculate

$$\begin{aligned} B(x, k_m, t) &= \sum_{n=-N}^N [H_n \delta\psi(x, \alpha n, t)] e^{2\pi i \frac{mn}{2N}}, \quad m = -N + 1, \dots, N, \\ B(x, k_{-N}, t) &= \sum_{n=-N}^N [H_n \delta\psi(x, \alpha n, t)] e^{-in\pi} \end{aligned} \quad (16)$$

via inverse FFT program as

$$B(x, k_m, t) = \sum_{n=0}^{2N-1} S_n e^{2\pi i \frac{mn}{2N}} + H_{-N} \delta\psi(x, \alpha n, t) e^{-in\pi}, \quad m = -N + 1, \dots, N, \quad (17)$$

where  $S_n = H_n \delta\psi(x, \alpha n, t)$  and  $S_n = S_{n-2N}$  ( $n = N + 1, \dots, 2N - 1$ ).

Now the Wigner equation (7) is simply approximated by collocations at the appropriate equally space nodes,

$$\partial_t w_N(x, k_m, t) + k_m \cdot \nabla_x w_N(x, k_m, t) + B(x, k_m, t) = Q(w_N(x, k_m, t)). \quad m = -N, \dots, N \quad (18)$$

This section ends with several discussions about numerical methods for scattering term and discontinuous potential. In general, the relaxation time model can be handled by numerical integration techniques, while the Fokker-Planck model handled by Monte Carlo method or any numerical scheme for parabolic equations.

As the Wigner distribution is now approximated by a  $L^2$ -periodic function, the aliasing error induced by the interactions between the original function and its artificial images in  $L^2$ -space should be handled carefully. Sufficient smoothness of  $w$  and  $V$  is required so that the aliasing error will decay rapidly on the boundary of the computational domain [6, 21]. However, the above requirements are not necessarily satisfied, as potential function may have some gaps (for instance, the barriers in semiconductors) [22]. This problem can be partially resolved by artificially splitting the potential into two parts, namely,  $V = V^{barrier} + V^{self}$ , where  $V^{barrier}$  is a discontinuous barrier potential, and  $V^{self}$  is the self-consistent electrostatic field. Hence, the smooth part  $V^{self}$  can be tackled by the spectral collocation method, while the non-smooth barrier potential by numerical integration techniques.

## B. A multistep scheme for the hyperbolic systems

The remaining part is to discuss a numerical solver for the hyperbolic system (18). The multistep scheme is derived by observing that the initial-value problem (18) can be represented as an abstract ODE (or a mild solution), under the operator semigroup theory.

For a fixed  $k_m$ , denote by  $A = k_m \cdot \nabla_x$  and  $T(t) = e^{-tA}$  the operator semigroup generated by  $A$  in the Banach space  $\mathbb{X}$ . Since  $A$  is a symmetric operator,  $T(t)$  is a  $C_0$ -semigroup [23].

Now we seek a solution  $w_N \in C^1([0, T], \mathbb{X} \times \mathbb{K})$ . Rewrite Eq.(18) in its integrated form,

$$w_N(x, k_m, t) = T(t) w_N(x, k_m, 0) - \int_0^t ds T(t-s) [B(x, k_m, s) - Q(w_N(x, k_m, s))]. \quad (19)$$

Since  $T(t)x = x - k_m t$ , it yields

$$w_N(x, k_m, t + \Delta t) = w_N(x - k_m \Delta t, k_m, t) - \int_t^{t+\Delta t} ds [B - Qw_N](x - k_m(t + \Delta t - s), k_m, s). \quad (20)$$

To derive a numerical scheme for Eq.(20), a direct choice is to use interpolation or extrapolation polynomials to estimate the integral, using the same idea as the Adams multistep methods in solving ODEs [24].

Denote by  $g_m(x, s; t_{n+1}) = T(t_{n+1} - s)[B - Qw_N(x, k_m, s)]$ , where the subindex  $m$  of  $g_m(x, s; t_{n+1})$  indicates that  $T(t)$  is generated by the operator  $k_m \cdot \nabla_x$ . Assume  $g_m(x, s; t_{n+1}) \in C(\mathbb{X} \times \mathbb{K}, [0, t_{n+1}])$ , then  $g_m(x, t_{n+1}; t_{n+1})$  can be approximated by an extrapolation polynomial  $p(x, k_m, t)$  on nodes  $t_n, t_{n-1}, \dots, t_{n-p}$ , which is expressed in terms of backward differences,

$$\nabla^0 g_m(x, t_n; t_{n+1}) = g_m(x, t_n; t_{n+1}), \quad \nabla^{j+1} g_m(x, t_n; t_{n+1}) = \nabla^j g_m(x, t_n; t_{n+1}) - \nabla^j g_m(x, t_{n-1}; t_{n+1}), \quad (21)$$

as follows:

$$p(x, k_m, t) = p(x, k_m, t_n + s\Delta t) = \sum_{j=0}^{k-1} (-1)^j \binom{-s}{j} \nabla^j g_m(x, t_n; t_{n+1}). \quad (22)$$

Inserting Eq.(22) into Eq.(20), we arrive at the generalized Adams methods for solving the hyperbolic systems Eq.(18). We denote  $\tilde{w}_N$  the numerical solution of  $w$ .

**Algorithm 3.1** *Explicit Adams methods*

$$\begin{aligned} p = 0 : \quad & \tilde{w}_N(x, k_m, t_{n+1}) = \tilde{w}_N(x - k_m \Delta t, k_m, t_n) - \Delta t [\tilde{B} - Q\tilde{w}_N](x - k_m \Delta t, k_m, t_n), \\ p = 1 : \quad & \tilde{w}_N(x, k_m, t_{n+1}) = \tilde{w}_N(x - k_m \Delta t, k_m, t_n) - \frac{3}{2} \Delta t [\tilde{B} - Q\tilde{w}_N](x - k_m \Delta t, k_m, t_n) \\ & + \frac{1}{2} \Delta t [\tilde{B} - Q\tilde{w}_N](x - 2k_m \Delta t, k_m, t_{n-1}), \\ p = 2 : \quad & \tilde{w}_N(x, k_m, t_{n+1}) = \tilde{w}_N(x - k_m \Delta t, k_m, t_n) - \frac{23}{12} \Delta t [\tilde{B} - Q\tilde{w}_N](x - k_m \Delta t, k_m, t_n) \\ & + \frac{16}{12} \Delta t [\tilde{B} - Q\tilde{w}_N](x - 2k_m \Delta t, k_m, t_{n-1}) - \frac{5}{12} \Delta t [\tilde{B} - Q\tilde{w}_N](x - 3k_m \Delta t, k_m, t_{n-2}). \end{aligned} \quad (23)$$

Similarly, the integral can be approximated by interpolation polynomials, yielding

**Algorithm 3.2** *Implicit Adams methods*

$$\begin{aligned} p = 0 : \quad & \tilde{w}_N(x, k_m, t_{n+1}) = \tilde{w}_N(x - k_m \Delta t, k_m, t_n) - \frac{1}{2} \Delta t [\tilde{B} - Q\tilde{w}_N](x, k_m, t_{n+1}) \\ & - \frac{1}{2} \Delta t [\tilde{B} - Q\tilde{w}_N](x - k_m \Delta t, k_m, t_n), \\ p = 1 : \quad & \tilde{w}_N(x, k_m, t_{n+1}) = \tilde{w}_N(x - k_m \Delta t, k_m, t_n) - \frac{5}{12} \Delta t [\tilde{B} - Q\tilde{w}_N](x, k_m, t_{n+1}) \\ & - \frac{8}{12} \Delta t [\tilde{B} - Q\tilde{w}_N](x - k_m \Delta t, k_m, t_n) + \frac{1}{12} \Delta t [\tilde{B} - Q\tilde{w}_N](x - 2k_m \Delta t, k_m, t_{n-1}). \end{aligned} \quad (24)$$

Implicit Adams methods are not so practical in solving the hyperbolic systems (18) directly, but they can be used to correct the predicted value of  $w$  through explicit methods, known as the prediction-correction scheme.

Numerical methods of higher order can be derived in a similar way. To guarantee the consistency and stability of the numerical scheme, the coefficients should satisfy the root condition and certain algebraic relations [24].

The generalized Adams methods are devised for an initial-value problem, without any assumption of boundary conditions. Therefore, one can have more freedom to choose a formulation of the boundary condition, or simply make a nullification outside the computational domain. In addition, the Adams methods can be easily adapted in arbitrary dimension, owing to the way of approximating an integral with respect to time variable.

Another remarkable feature of multistep methods is that they track the Lagrangian advection in  $x$ -direction, resulting from the operator  $T(t)$ . Therefore the above methods, which make use of the backwards characteristics to construct extrapolation (or interpolation) functions, are just extensions of semi-Lagrangian scheme. The multistep methods are expected to be free from the restriction of Courant number and allow a longer time step, since they exploit the exact Lagrangian advection.

The price to pay is to reconstruct a regular grid using cubic spline interpolation. For the Wigner problem, it is relatively easy since the characteristic of  $w_t + k \cdot \nabla_x w = 0$  can be solved exactly. It is recommended to sample grid points along the characteristic line, so that the grid mesh obtains as many shifted grid points as possible. In general, we can choose  $\Delta x$  as  $\Delta x = N_x (\Delta k \cdot \Delta t)$ , where  $N_x$  indicates the numerical resolution. When the characteristic end is not lying on the grid mesh, it can be computed by cubic spline interpolation. (As illustrated in [16], the linear interpolation is too dissipative to be used, also shown in Section 4.) We call the numerical resolution is sufficiently high if  $N_x = 1$ , as the grid mesh contains all the sampled points except those deviating from the computational domain.

When explicit methods or prediction-correction methods are employed, all the calculations (including interpolation function, tensor matrix  $B$  and collision term  $Q$ ) can be carried out independently, thereby allowing an easy strategy for parallel and distributed computing. Thus, it is expected that multistep method are much more advantageous in high dimensional problem and High Performance Computing (HPC) environment, just like the semi-Lagrangian methods.

The multistep scheme requires more initial values to start up, which can be obtained from one-step methods, like FDMs and operator splitting scheme, with a smaller time step. However, the implementation of one-step methods usually requires some information of boundary condition. An alternative way is introduced to overcome this problem, by using the explicit backward Euler method (the first formula in Algorithm 3.1) for prediction and the implicit mid-point Euler method (the first formula in Algorithm 3.2) for correction, with a smaller time step.

### C. Boundary conditions

So far we have not discussed the boundary conditions yet. In principle, the formulation of boundary conditions is not necessary in the multistep methods, since they are devised to tackle a Cauchy problem. Nevertheless, the computational domain  $\Omega$  cannot be infinitely large and needs a reasonable truncation. When the computational domain is not large enough, it is also necessary to introduce a boundary condition. Or a simple nullification can be made outside the domain, with a Dirichlet boundary condition  $w = 0$  on  $\partial\Omega$ .

The boundary conditions in open quantum systems and corresponding mathematical concepts have been



Table 1: Units and parameters.

Physical quantity	Unit	Value
Time	$fs$	-
Length	$nm$	-
Energy	$eV$	-
Temperature	$K$	-
Electron mass $m_e$	$eV \cdot fs^2 \cdot nm^{-2}$	5.68562966
Planck constant $\hbar$	$eV \cdot fs$	0.658211899
Boltzmann constant $k_B$	$eV \cdot K^{-1}$	$8.61734279 \times 10^5$

illustrated in [5, 14]. We only review the well-known inflow boundary conditions, proposed by Frenslley,

$$\begin{aligned} w(x_L, k, t) &= w_L(x_L, k), \quad k > 0, \\ w(x_R, k, t) &= w_R(x_R, k), \quad k < 0, \end{aligned} \tag{25}$$

where  $w_L(k, t)$  and  $w_R(k, t)$  can be approximated by Fermi-Dirac distribution.

Solving the Wigner-Poisson equation is much more complicated due to the coupling self-consistent Poisson equation. In principle, the multistep scheme can tackle the nonlinear problems, like its counterpart in numerical ODEs. However, a boundary condition, which asymptotically conserves the charge neutrality in the quantum system, is necessary for solving the Poisson equation [5]. In previous papers, a time-dependent Dirichlet boundary condition was introduced [26], although its validation was not illustrated. In the next section, we only focus on the linear Wigner equation. The self-consistent field will be discussed in subsequent papers.

## 4 Numerical results

### A. Test problems

The numerical results are presented by simulating the motion of a Gaussian wave packet (GWP) in several barrier potentials, which have been studied in [4, 9, 26]. To facilitate a comparison, the author uses the same physical units and quantities as in [4, 9], listed in Table 1.

The purpose of numerical tests is twofold. First, we test the accuracy and convergence of multistep methods through a comparison between the first-order upwind finite difference method and the explicit multistep method. The performance metric is based on either the exact solutions or numerical solutions with high resolution ( $N_x = 1, \Delta t = 0.05$ ). The second purpose is to investigate the quantum tunneling effect of the Wigner distribution in the free space and to discuss the influence of scattering effects, where the scattering process is modeled by the relaxation time model.

The rescaled collisionless Wigner equation in one dimension is

$$\frac{\partial w}{\partial t} + \frac{\hbar k}{m} \frac{\partial w}{\partial x} + \frac{1}{2\pi\hbar} \theta[V] w = 0. \tag{26}$$

When including the scattering effect, it yields the collisional Wigner equation

$$\frac{\partial w}{\partial t} + \frac{\hbar k}{m} \frac{\partial w}{\partial x} + \frac{1}{2\pi\hbar} \theta[V] w = \frac{1}{\tau} \left( \frac{n}{n_0} w_0 - w \right). \quad (27)$$

The wave function of a GWP is expressed as

$$\psi(x, t) = \left[ \frac{1}{2\pi\alpha^2 (1 + i\beta t)^2} \right]^{\frac{1}{4}} e^{i(k_0 x - \omega_0 t)} \exp \left[ -\frac{(x - v_0 t)^2}{4\alpha^2 (1 + i\beta t)} \right], \quad (28)$$

where  $v_0$  is the average velocity,  $\alpha$  is the minimum position spread, and

$$\beta = \frac{\hbar}{2m\alpha^2}, \quad v_0 = \frac{\hbar k_0}{m} = \frac{2\omega_0}{k_0}. \quad (29)$$

The Wigner-function description of Eq.(28) is

$$w(x, k, t) = 2 \exp \left\{ -\frac{(x - x_0 - v_0 t)^2}{2\alpha^2 (1 + \beta^2 t^2)} \right\} \exp \left\{ -2\alpha^2 (1 + \beta^2 t^2)^2 \left[ (k - k_0) - \frac{\beta t (x - x_0 - v_0 t)}{2\alpha^2 (1 + \beta^2 t^2)} \right]^2 \right\}, \quad (30)$$

which is the exact solution of (26) when  $V = 0$ .

The initial condition for the GWP simulation is

$$w(x, k, 0) = 2 \exp \left[ -\frac{(x - x_0)^2}{2\alpha^2} \right] \exp \left[ -2\alpha^2 (k - k_0)^2 \right]. \quad (31)$$

The quantum tunneling effect is investigated by simulating a GWP hitting a Gaussian barrier with three different heights. The Gaussian barrier with a width  $\omega$  is given

$$V(x) = H \exp^{-\frac{x^2}{2\omega^2}}, \quad (32)$$

where the self-consistent electrostatic potential is not included. In subsequent simulations, the heights  $H$  of  $V(x)$  are chosen to be 0.3, 1.3 and 2.3, respectively, with  $\omega = 1$ .

If not specified, the coefficients in simulations are chosen as  $\alpha = 2.825$ ,  $m = 0.0665m_e$ ,  $x_0 = -30$  and  $k_0 = 1.4$  so that the kinetic energy of GWP is  $E_0 \approx 1.12$ . The computational domain  $\Omega = \mathbb{X} \times \mathbb{K}$  is  $\left[ -\frac{125\pi\hbar}{16m}, \frac{125\pi\hbar}{16m} \right] \times [-2\pi, 2\pi]$ , with  $\Delta x = \frac{\pi\hbar}{64m}$ ,  $\Delta k = \frac{\pi}{64}$ . The maximum  $\Delta t$  are chosen to be 0.2 (the Courant number is  $\sigma = \frac{\hbar\Delta t}{m\Delta x} = 4.08$ ).

For the multistep methods, the one-step prediction-correction method is used to obtain the missing starting points, with the same time step  $\Delta t = 0.05$ . The shifted grid points are interpolated by cubic spline interpolation if not lying on the grid mesh. And the boundary condition is chosen as the Dirichlet type,  $w = 0$  on  $\partial\Omega$ , with a nullification for the shifted grid points outside  $\Omega$ . While the inflow boundary condition is employed for the upwind finite difference method,

$$\begin{aligned} w(x_L, k, t) &= w(x_L, k, 0), \quad k > 0, \\ w(x_R, k, t) &= w(x_R, k, 0), \quad k < 0. \end{aligned} \quad (33)$$

The numerical error induced by the boundary conditions is negligible, as the computational domain  $\Omega$  is chosen large enough. In fact, it has  $w(x_L, k, 0) \approx 0$  and  $w(x_R, k, 0) \approx 0$ .

## B. Numerical results

In order to test the accuracy of multistep methods, a comparison is made between the multistep scheme and the upwind FDM by monitoring the error when simulating the time evolution of the GWP in the free space ( $V = 0$ ), without the collision term. The performance metrics are  $L^2$  error and  $L^\infty$  error [4],

$$\begin{aligned}\epsilon_2(t) &= \left[ \int_{\mathbb{X} \times \mathbb{K}} (\Delta w(x, k, t))^2 dx dk \right]^{\frac{1}{2}}, \\ \epsilon_\infty(t) &= \max \{ \Delta w(x, k, t) \}, \quad (x, k) \in \mathbb{X} \times \mathbb{K},\end{aligned}\tag{34}$$

where  $\Delta w(x, k, t) = |w^{reference}(x, k, t) - w^{num}(x, k, t)|$ . In practice,  $\epsilon_2$  is approximated by

$$\bar{\epsilon}_2(t) = \left[ \sum_{\mathbb{X} \times \mathbb{K}} (\Delta w(x, k, t))^2 \Delta x \Delta k \right]^{\frac{1}{2}}.\tag{35}$$

The evolution of a GWP in the free space ( $V = 0$ ) is simulated by both methods with the same time step  $\Delta t = 0.05$ . In this case, the multistep scheme reduces to

$$\tilde{w}_N(x, k_m, t_{n+1}) = \tilde{w}_N\left(x - \frac{\hbar}{m} k_m \Delta t, k_m, t_n\right),\tag{36}$$

which is the exact solution of  $\partial_t w + \frac{\hbar}{m} k_m \nabla_x w = 0$ . Numerical results are listed as follows.

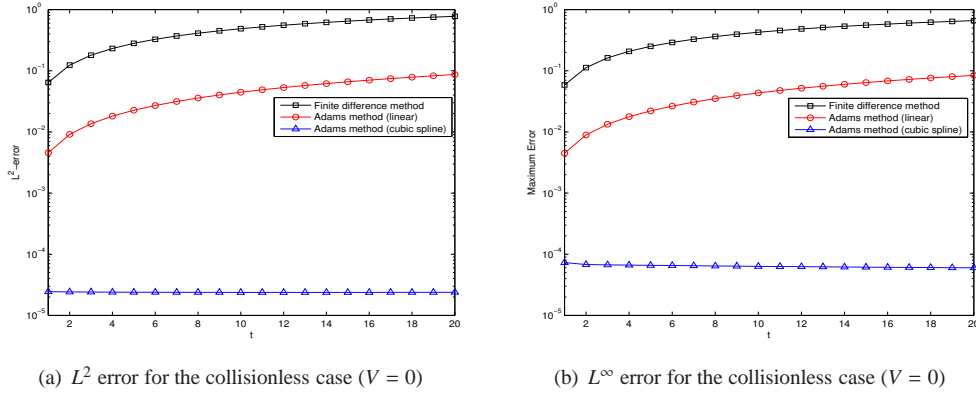


Figure 1: Numerical error of Wigner functions in the flat potential ( $V = 0$ )

We have tested both linear interpolation method and cubic spline interpolation method. It is demonstrated in Figure 1 that interpolation methods are far more accurate than the FDM, since the FDM suffers from the dissipative error, while the numerical error in the Adams method only results from the interpolation polynomials. It is also shown that the numerical error of linear interpolation is significantly larger than cubic spline interpolation. Actually, numerical dissipation is still observed in linear interpolation method.

Figure 2c shows the distribution of the numerical error  $\Delta w$  of cubic interpolation method at  $t = 20$ , which yields a very precise result. In Figure 2d we make a comparison of numerical waveforms at  $k = 1.3744$ ,  $t = 20$ . The linear interpolation method yields a slight different waveform, which accords with the observation of [16].

Therefore, in the following simulations, we only employ cubic spline interpolation to compute the shifted grid points.

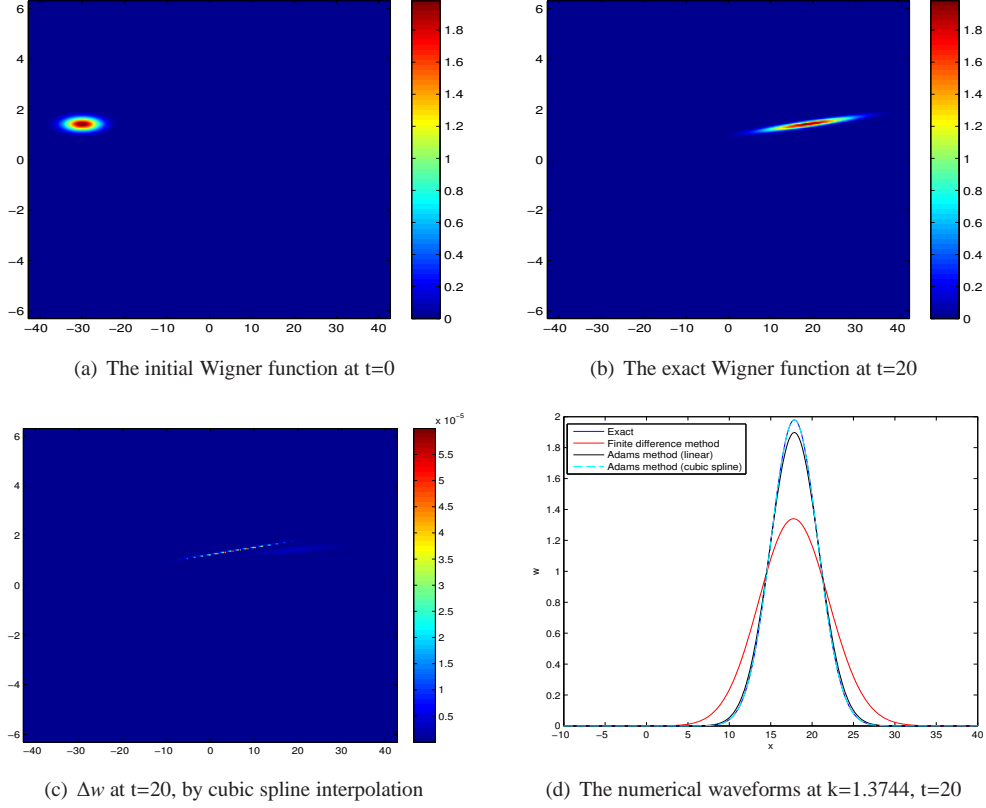


Figure 2: The Wigner function in the free space ( $V = 0$ )

We let a GWP with kinetic energy  $E_0 \approx 1.12$  to hit several Gaussian barriers. The explicit three-step method is employed, combining with the spectral collocation method to discretize the pseudo-differential operator. The choice of Gaussian potential guarantees the consistency and convergence of the spectral collocation method.

To show the convergence of multistep methods, we choose  $H$  to be 1.3 and monitor the  $L^2$  and  $L^\infty$  error under three time steps. Since the exact solution of Eq. (26) is not trivial, we choose the numerical solution with  $\Delta t = 0.05$  and high resolution  $N_x = 1$  as a reference. It is shown in Figure 3 that numerical errors are significantly small in a short time, since free advection is dominant. Afterwards quantum interference becomes important and larger numerical errors are observed. As shown in Figure 3, numerical errors are reduced dramatically when the time step becomes smaller. The numerical errors resulting from the cubic spline interpolation are less than  $10^{-3}$  (the line  $\Delta t = 0.05$ , where  $N_x = 20$ ), which demonstrates its accuracy.

Figure 4 shows the Wigner function for the GWP interacting with the Gaussian barrier  $V(x) = 0.3e^{-\frac{x^2}{2}}$ . The kinetic energy  $E_0$  of GWP is much greater than the barrier height. Therefore, the GWP travels across the barrier easily, with only a slight change of the waveform.

If the height of barrier is comparable to  $E_0$ , the GWP is separated into two wave packets due to the quantum

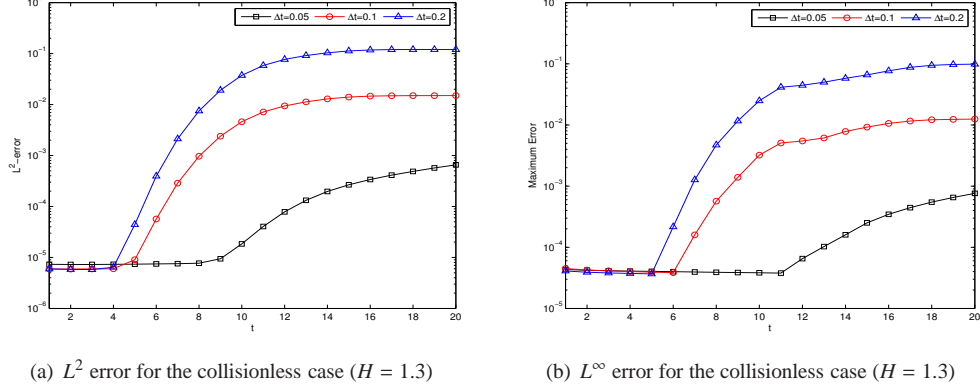


Figure 3: Numerical error of Wigner functions in a Gaussian barrier ( $H = 1.3$ )

interference with the Gaussian barrier. Although the kinetic energy is smaller than the barrier height, one part of the wave is still able to travel across the barrier, while another is reflected back, seen in Figure 5.

When the height of potential barrier grows larger, like  $H = 2.3$ , the GWP is almost completely reflected back, seen in Figure 6.

We turn to the collisional Wigner equation. The exact solution of Eq.(27) is also not trivial, even with a flat potential. For a special case, the analytical solution can be solved by separation of variables. Assume the wave (the Wigner distribution) moves in a uniform velocity  $v_0 = \frac{\hbar k_0}{m}$  under a flat potential  $V = 0$ , then the corresponding Wigner equation is

$$\frac{\partial w}{\partial t} + \frac{\hbar k_0}{m} \frac{\partial w}{\partial x} = \frac{1}{\tau} \left( \frac{n}{n_0} w_0 - w \right). \quad (37)$$

It is easy to verify that the exact solution of Eq.(37) is

$$w(x, k, t) = 2 \exp \left[ -\frac{(x - x_0 - v_0 t)^2}{2\alpha^2} \right] \exp \left[ -2\alpha^2 (k - k_0)^2 \right]. \quad (38)$$

The collision term involves an integral  $n(x, t) = \int w(x, k, t) dk$ , which can be approximated by the composite Simpson rule at the nodes  $k_{-N}$  to  $k_N$ ,

$$n(x, t) = \frac{\Delta k}{3} \left( f(x, k_{-N}, t) + f(x, k_N, t) + 4 \sum_{i=1}^N f(x, k_{2i-1-N}, t) + 2 \sum_{i=1}^{N-1} f(x, k_{2i-N}, t) \right). \quad (39)$$

In this case, the accuracy of explicit three-step method is shown in Figure 7, with time step  $\Delta t = 0.05$  and  $N_x = 20$ .

To make a further investigation of the convergence and robustness of Adams multistep scheme, a comparison is made between numerical results with different time steps or different numerical resolutions. The relaxation time  $\tau$  is chosen 1. We choose the same performance metrics,  $L^2$ -error and  $L^\infty$ -error, to monitor the numerical errors.

As shown in Figure 8, the Adams method gives accurate numerical results, while the time step  $\Delta t = 0.1$  seems to yield the best numerical result. It is because of the numerical errors come from both cubic spline

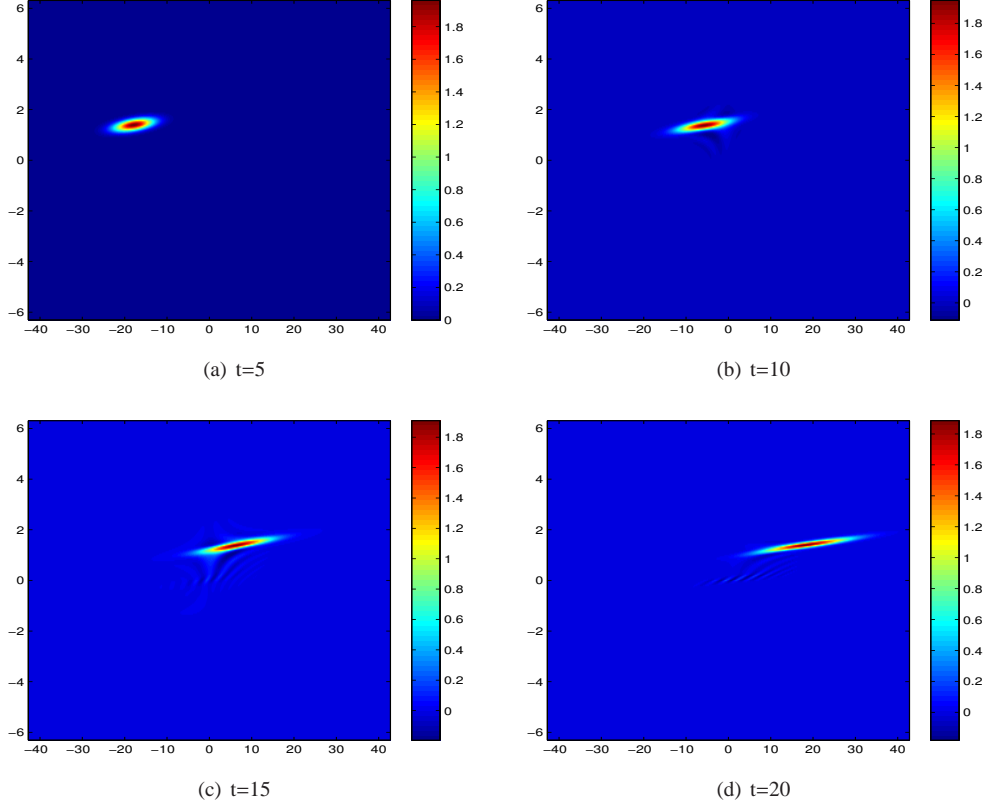


Figure 4: The Wigner function of the GWP interacting with a Gaussian barrier ( $H = 0.3$ )

interpolation and numerical integration. A larger time step may increase the global error in  $t$ -direction, but it needs less interpolated grid points, thereby reducing the possible numerical error resulting from interpolations simultaneously. Therefore, an appropriate time step is chosen to strike a balance between accuracy and efficiency.

The numerical resolution is also discussed, seen in Figure 9, where the time step is chosen to be 0.1. The accuracy is tested and the convergence trend is very clear. In this case, the lowest resolution  $N_x = 20$  gives the best numerical results, since the numerical error mainly comes from the discrete approximation of collisional term. Hence, this test makes us confident that a relatively low numerical resolution can be chosen to achieve the efficiency, without too much loss of accuracy.

Now we include the quantum interference in the model and discuss how the scattering process influences the quantum tunneling effect, by solving Eq.(27) numerically. We let a GWP hit a Gaussian barrier  $V(x) = 2.3e^{-\frac{x^2}{2}}$  and investigate the Wigner function under different relaxation time  $\tau$ .

We first investigate the convergence of Adam multistep scheme in the collisional case. The explicit three-step method is used, with different time step  $\Delta t = 0.05, 0.1, 0.2$ , respectively. The relaxation time  $\tau$  is chosen as 1 and numerical mesh is set as before. The numerical solutions with  $\Delta t = 0.05$  and high resolution  $N_x = 1$  are chosen as the reference. When time step becomes smaller, an obvious error reduction is shown in Figure

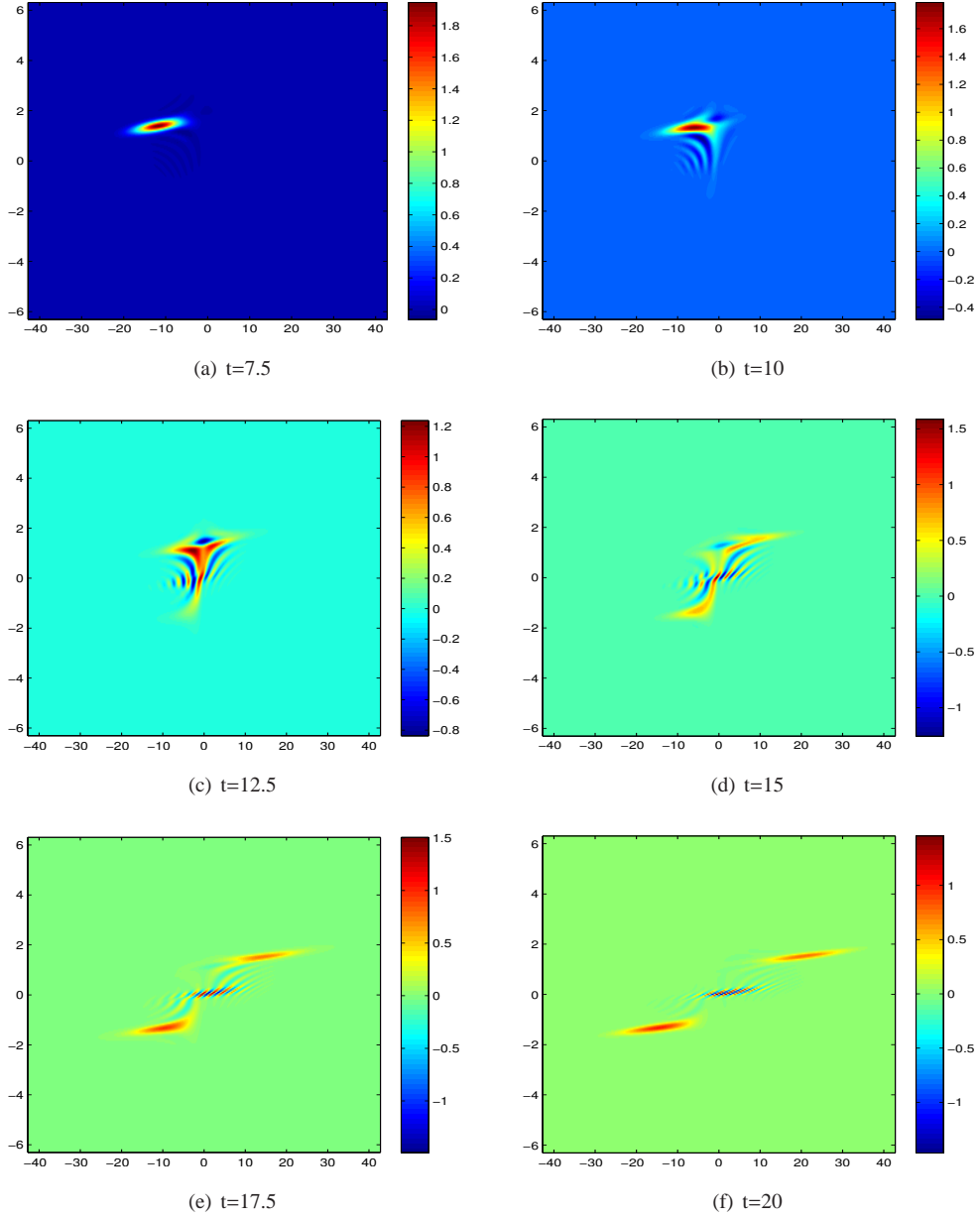


Figure 5: The Wigner function of the GWP interacting with a Gaussian barrier ( $H = 1.3$ )

10, indicating the convergence of the explicit three-step Adams method.

Finally, we give some information about the relaxation time model. If the relaxation time  $\tau$  is sufficiently large, a weak dissipation is expected. On the other hand, when the dissipation is strong enough (for a small  $\tau$ ), it's easy for the perturbed Wigner function to return into its equilibrium state. When  $\tau$  is chosen as 1, it is observed in Figure 11 that the Wigner function nearly preserves its waveform even after a quantum mechanical interaction with a high barrier potential.

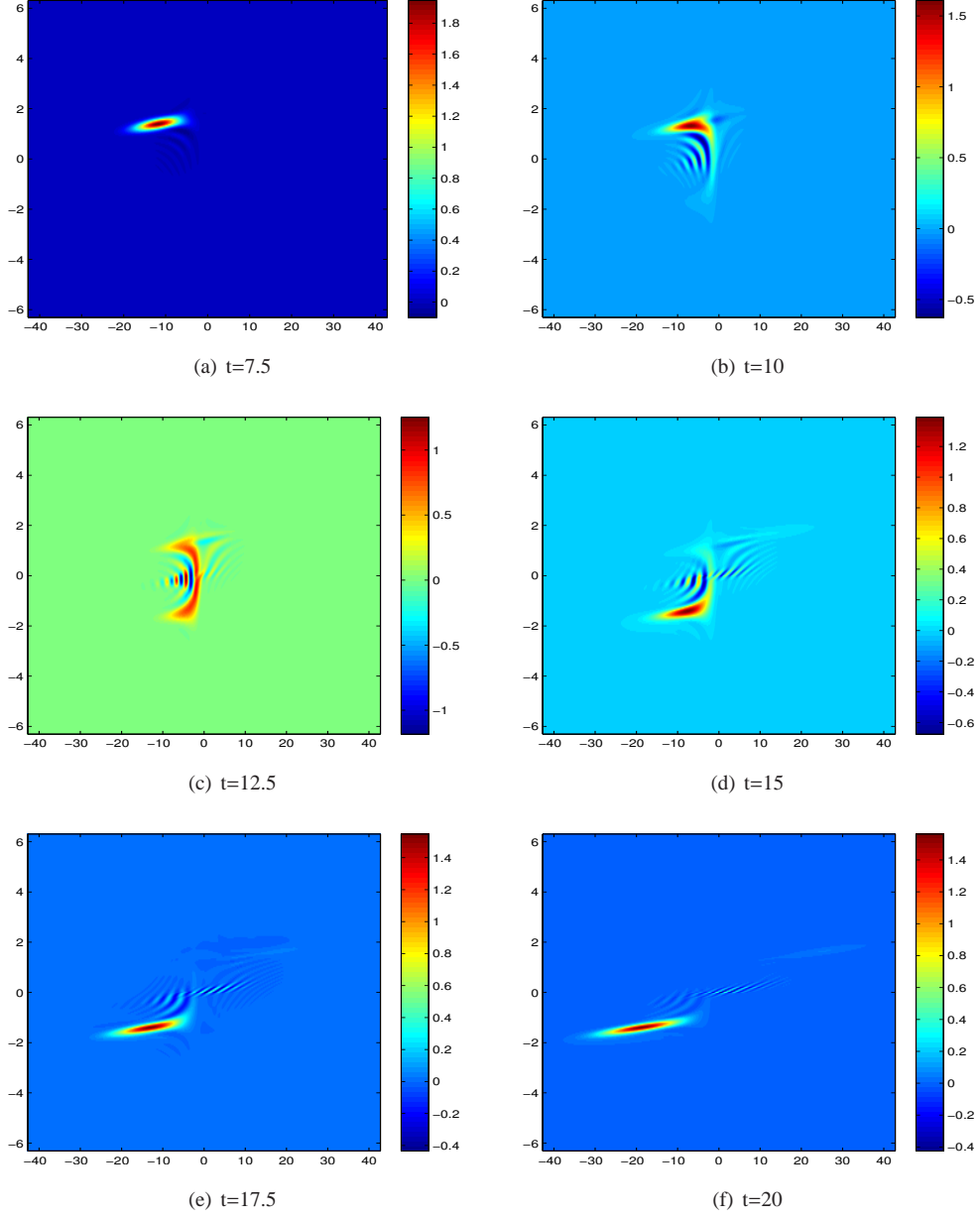


Figure 6: The Wigner function of the GWP interacting with a Gaussian barrier ( $H = 2.3$ )

As the relaxation time  $\tau$  grows larger, the quantum effect becomes more obvious. Figure 12 shows that under a weaker dissipation ( $\tau = 3$ ), the wave is still able to travel across a high barrier potential partly, while another is reflected back. Since the relaxation time model forces the wave to return into its equilibrium, the reflected wave presents two streams.

When the relaxation time  $\tau$  is chosen as 10, the quantum effect is dominant and the wave is expected to be reflected back in a similar way as the collisionless case. It is observed in Figure 12 that the reflected wave also



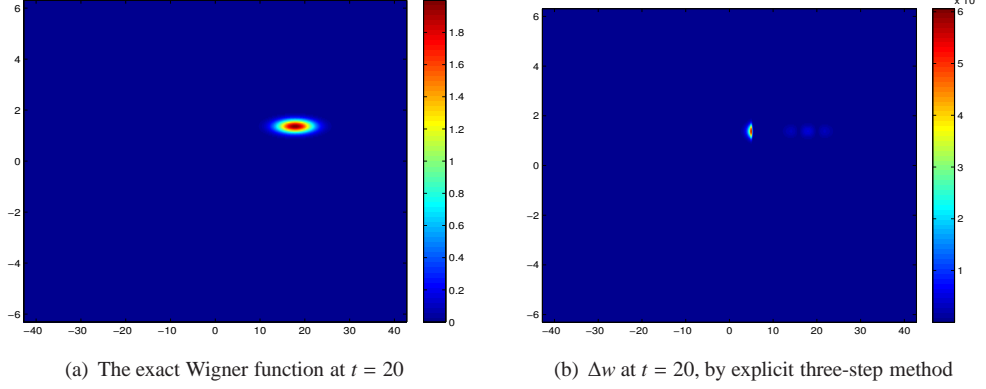


Figure 7: Numerical error of the Wigner function in the collisional case ( $\tau = 1, V = 0$ )

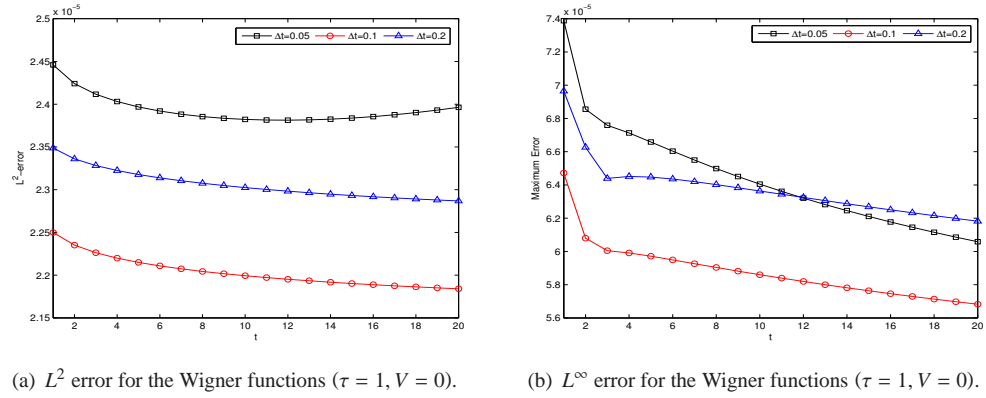


Figure 8:  $L^2$  and  $L^\infty$  error of the Wigner function, with different time steps.

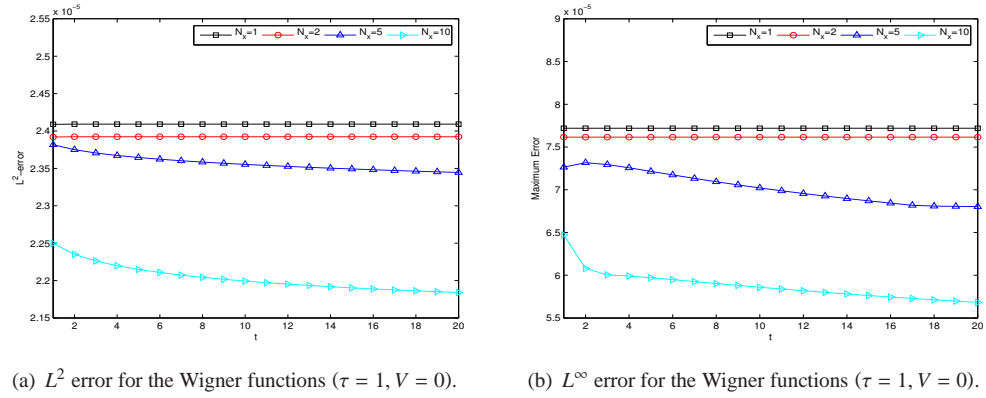


Figure 9:  $L^2$  and  $L^\infty$  error of the Wigner function, with different numerical resolutions.

separates into two streams, due to the mixing of quantum effect and scattering effect.

This section ends with a final remark. In the above simulation, the electron-phonon interaction is modeled

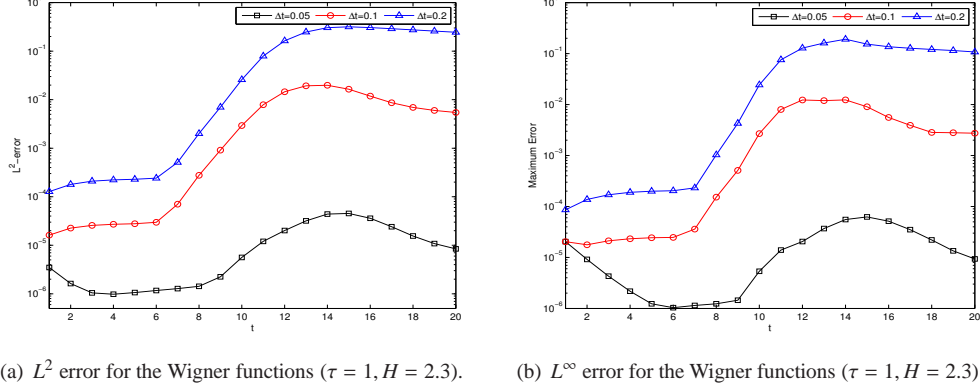


Figure 10: Numerical error of Wigner functions in a Gaussian barrier ( $H = 2.3$ ), with relaxation time  $\tau = 1$

with classical relaxation time model, which effectively removes the correlation and introduces irreversibility [26]. However, the tunneling in this model may be generated by some approximate scattering mechanism. To evaluate the scattering effect more properly, it necessitates a modification of the collisional Wigner equation, including scattering process quantum mechanically. We wish to discuss it in subsequent papers.

## 5 Conclusions

In this paper, we mainly discuss a multistep scheme of solving the initial-value Wigner equation. It exploits the property of operator semigroup generated by the hyperbolic operator  $k \cdot \nabla_x$  and deal with the Lagrangian advection more properly than the FDMs. Besides, the time step in explicit multistep scheme is not restricted by Courant-Friedrichs-Lévy condition, which has been validated in numerical simulations. Since it is devised to tackle a Cauchy problem, the multistep scheme may avoid some unphysical effects induced by artificial boundary conditions, while it is also compatible with various of formulations of boundary conditions.

The spectral collocation method is used to discretize the pseudo-differential operator  $\theta$ . Owing to FFTs, the cost of calculating  $\theta$  can be reduced dramatically, therefore it is an efficient way to solve the high-dimensional problem. The weakness of spectral method is that its consistency and convergence is strongly related to smoothness of  $w$  and  $V$ , which can be partially resolved by artificially splitting the Wigner potential into a smooth part and a non-smooth part, where the smooth potential is tackled by spectral methods. Numerical integration technique is used to deal with the collision operator  $Q(w)$  and its consistency is verified by numerical simulations.

The author omits the detailed discussion about self-consistent field in numerical simulations since it is quite difficult to formulate an appropriate boundary condition for solving the Poisson equation. It is pointed out that the multistep methods can be easily generalized to the nonlinear case, like the multistep ODE solvers. The author wishes to discuss the self-consistent quantum effect, along with a more proper treatment of collision operator, in subsequent papers.

**Acknowledgements** The author would like to thank Dr. Huasheng Xie and Professor Yong Xiao in the IFTS, Zhejiang University, for discussions on kinetic theory and transport equation.

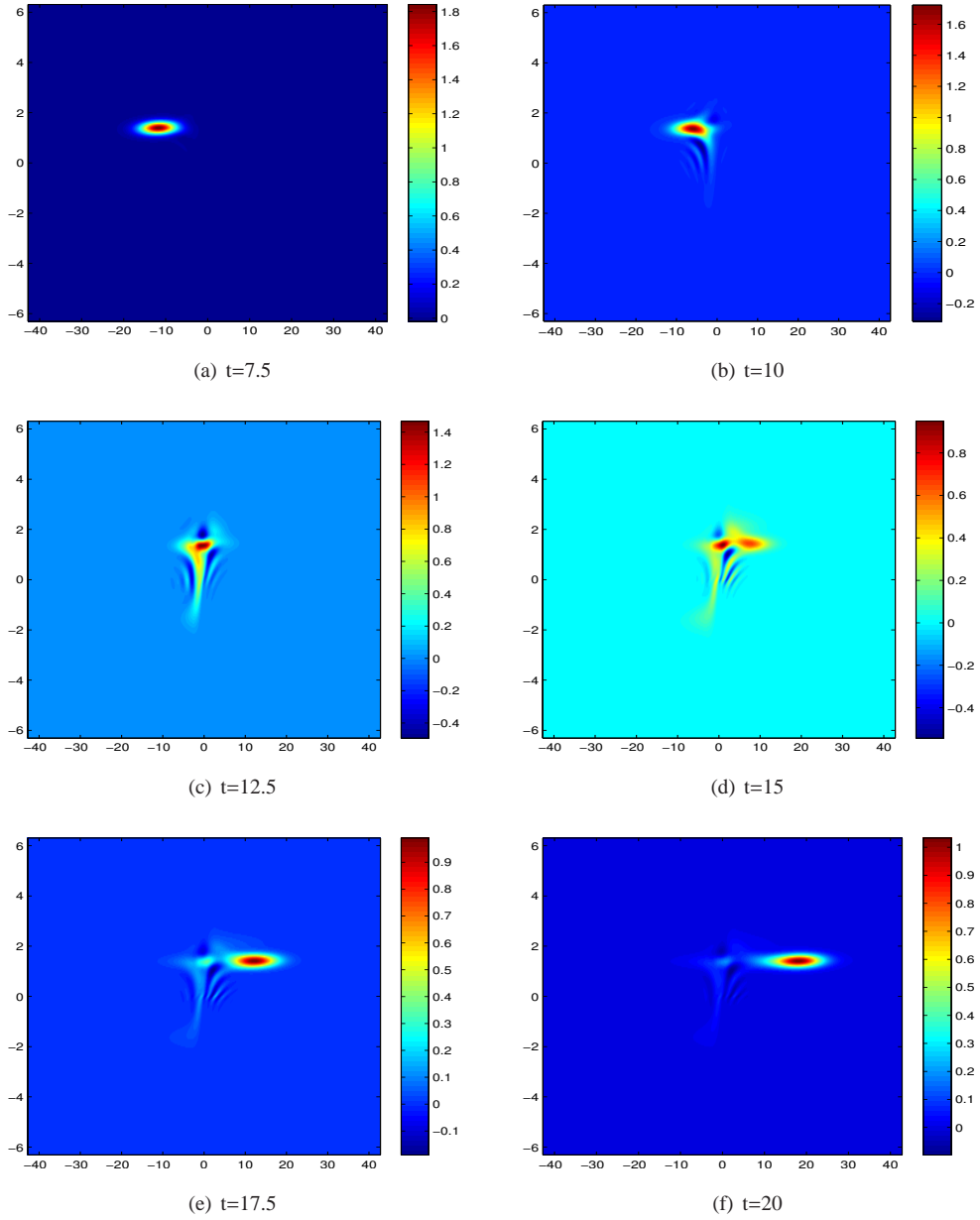


Figure 11: The Wigner function for the GWP interacting with a Gaussian barrier ( $H = 2.3, \tau = 1$ )

## References

- [1] Ringhofer C. Computational methods for semiclassical and quantum transport in semiconductor devices. *Acta Numerica*, 1997, 6: 485-521.
- [2] Wigner E. On the quantum correction for thermodynamic equilibrium. *Physical Review*, 1932, 40(5): 749.

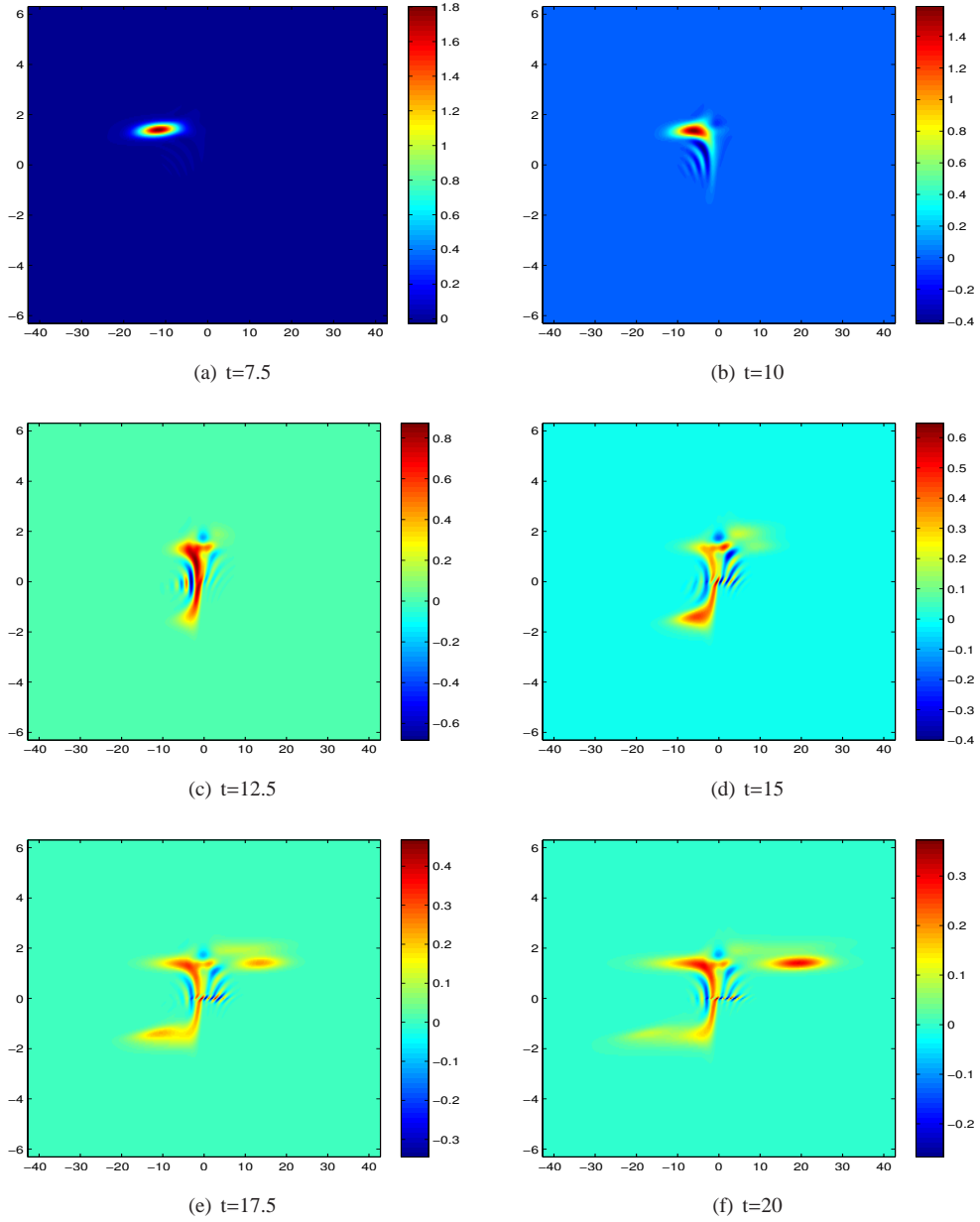


Figure 12: The Wigner function for the GWP interacting with a Gaussian barrier ( $H = 2.3, \tau = 3$ )

- [3] Tatarski V I. The Wigner representation of quantum mechanics. Soviet Physics Uspekhi, 1983, 26(4): 311.
- [4] Shao S, Lu T, Cai W. Adaptive conservative cell average spectral element methods for transient Wigner equation in quantum transport. Communication in Computational Physics, 2011, 9(3): 711-739.
- [5] Frensley W R. Wigner-function model of a resonant-tunneling semiconductor device. Physical Review B, 1987, 36(3): 1570.

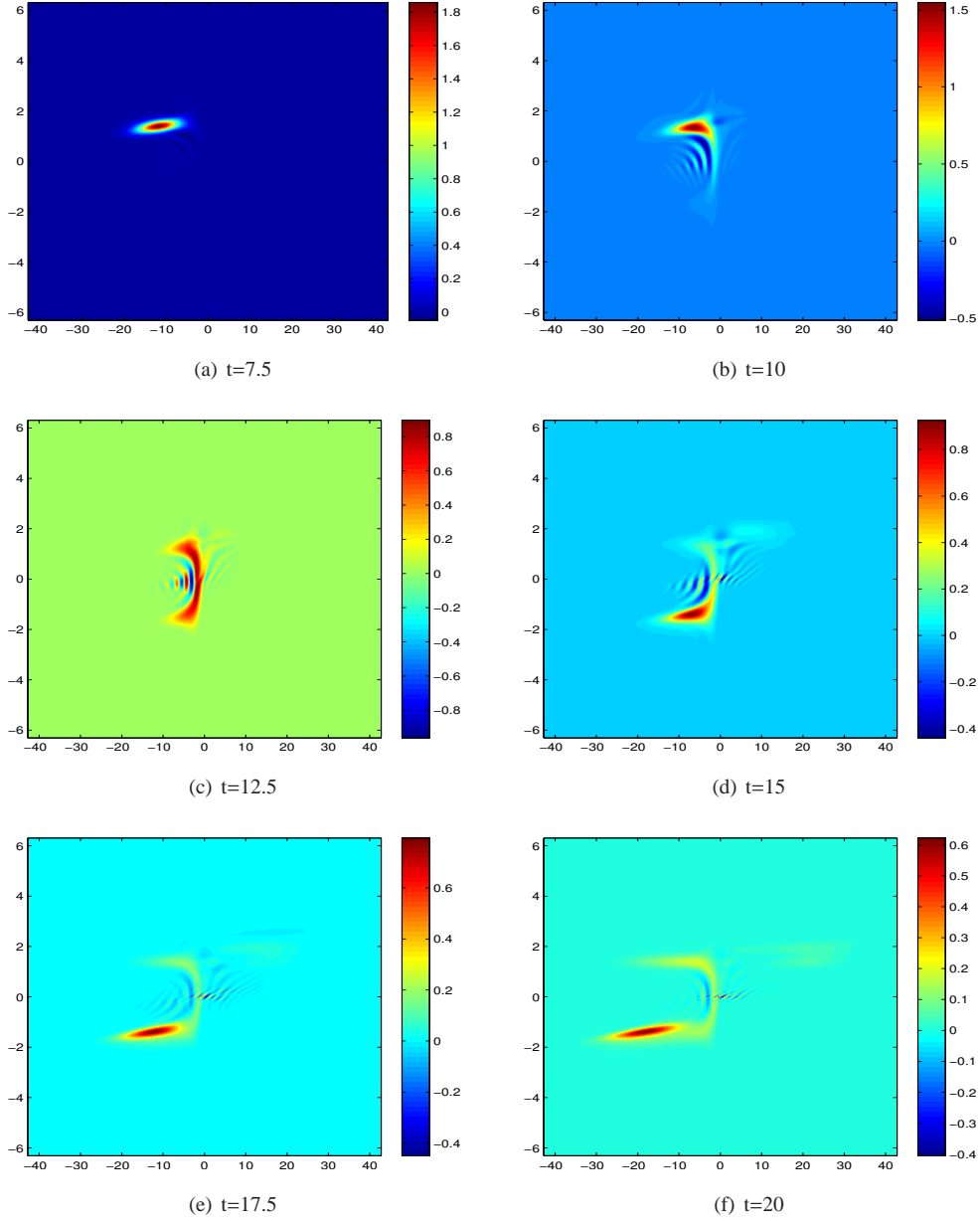


Figure 13: The Wigner function for the GWP interacting with a Gaussian barrier ( $H = 2.3, \tau = 10$ )

- [6] Ringhofer C. A spectral method for the numerical simulation of quantum tunneling phenomena. *SIAM Journal on Numerical Analysis*, 1990, 27(1): 32-50.
- [7] Suh N D, Feix M R, Bertrand P. Numerical simulation of the quantum Liouville-Poisson system. *Journal of Computational Physics*, 1991, 94(2): 403-418.
- [8] Arnold A, Ringhofer C. An operator splitting method for the Wigner-Poisson problem. *SIAM journal on numerical analysis*, 1996, 33(4): 1622-1643.

- [9] Biegel B A. Quantum electronic device simulation. Stanford University, 1997.
- [10] Sellier J M, Dimov I. A sensitivity study of the Wigner Monte Carlo method. *Journal of Computational and Applied Mathematics*, 2015, 277: 87-93.
- [11] Sellier J M, Dimov I. A Wigner Monte Carlo approach to density functional theory. *Journal of Computational Physics*, 2014, 270: 265-277.
- [12] Shifren L, Ferry D K. Particle Monte Carlo simulation of Wigner function tunneling. *Physics Letters A*, 2001, 285(3): 217-221.
- [13] Heitzinger C, Ringhofer C, Ahmed S, et al. 3D Monte-Carlo device simulations using an effective quantum potential including electron-electron interactions. *Journal of Computational Electronics*, 2007, 6(1-3): 15-18.
- [14] Arnold A. Numerically absorbing boundary conditions for quantum evolution equations. *VLSI design*, 1998, 6(1-4): 313-319.
- [15] Arnold A. Mathematical concepts of open quantum boundary conditions. *Transport Theory and Statistical Physics*, 2001, 30(4-6): 561-584.
- [16] Sonnendrücker E, Roche J, Bertrand P, Ghinzzo A. The semi-Lagrangian method for the numerical resolution of the Vlasov equation. *Journal of Computational Physics*, 1999, 149(2): 201-220.
- [17] Manfredi G. How to model quantum plasmas. *Fields Inst. Commun*, 2005, 46: 263-287.
- [18] Gantsevich S V, Gurevich V L, Katilius R. Fluctuations in semiconductors in a strong electric field and scattering of light by "hot" electrons. *Soviet Physics JETP*, 1970, 30: 276-284.
- [19] Glassey R T. *The Cauchy problem in kinetic theory*. SIAM, 1996.
- [20] Brezzi F, Markowich P A. The three-dimensional Wigner-Poisson problem: Existence, uniqueness and approximation. *Mathematical Methods in the Applied Sciences*, 1991, 14(1): 35-61.
- [21] Ringhofer C. On the convergence of spectral methods for the Wigner-Poisson problem. *Mathematical Models and Methods in Applied Sciences*, 1992, 2(01): 91-111.
- [22] Lasater M. *Numerical methods for the wigner-poisson equations*. 2005.
- [23] Renardy M, Rogers R C. *An introduction to partial differential equations*. New York: Springer, 2004.
- [24] Hairer E, Nørsett S P, Wanner G. *Solving ordinary differential equations I: nonstiff problems*. Springer Science and Business, 2008.
- [25] Frensley W R. Boundary conditions for open quantum systems driven far from equilibrium. *Reviews of Modern Physics*, 1990, 62(3): 745.
- [26] Klusdahl N C, Krivan A M, Ferry D K, et al. Self-consistent study of the resonant-tunneling diode. *Physical Review B*, 1989, 39(11): 7720.